Nuclear Materials and Energy 000 (2016) 1–5

Contents lists available at ScienceDirect

Nuclear Materials and Energy

journal homepage: www.elsevier.com/locate/nme

Sputtering properties of RAFM steels under high-flux He plasma exposure

D. Nishijima[a,*], M.J. Baldwin[a], R.P. Doerner[a], H. Tanigawa[b], P. Wang[c], J.H. Yu[a]

[a] Center for Energy Research, University of California at San Diego, 9500 Gilman Dr., La Jolla, CA 92093-0417, USA
[b] National Institutes for Quantum and Radiological Science and Technology, Rokkasho, Aomori 039-3212, Japan
[c] Lanzhou Institute of Chemical Physics, Chinese Academy of Sciences, No. 18, Tianshui middle road, Lanzhou, 730000, China

ARTICLE INFO

Article history:
Available online xxx

Keywords:
Reduced activation ferritic/martensitic steel
Sputtering
Spectroscopy

ABSTRACT

Sputtering properties of F82H and CLF-1 RAFM (reduced activation ferritic/martensitic) steels are investigated under exposure to high-flux He plasmas ($\Gamma_i \sim 2$–4×10^{22} m^{-2}s^{-1}) in PISCES-B with a low incident ion energy of ~80 eV and sample temperature, T_s, ranging from ~573 K to 1053 K. Both steels are primarily alloys of Fe, Cr, and W. While sputtered W atoms were not detected during the exposure, sputtered Fe and Cr atomic fluxes were spectroscopically quantified using *S/XB* values of Fe I and Cr I emission lines, which were experimentally determined in this study. Sputtering yields of F82H obtained from spectroscopy agree well with those from mass loss measurements. The He^+ fluence-integrated sputtering yield of F82H and CLF-1 does not depend on T_s in the range of ~573–873 K, but starts to increase at T_s ~900 K. Sputtered Fe and Cr atomic fluxes are found to drop during the plasma exposure. The reduction of sputtering yield is explained by surface enrichment of W and development of surface morphology. The surface enrichment of W was measured with Auger electron spectroscopy, and is due to the observed preferential sputtering of Fe and Cr. Cone-like structures were observed with a scanning electron microscope, which become larger with increasing T_s, and W fuzz is formed on top of the cones at $T_s \geq 973$ K.

1. Introduction

While reduced activation ferritic/martensitic (RAFM) steel is a promising candidate for structural material in future fusion reactors, its use as a first wall material is also considered an attractive option. Thus, investigations of RAFM steel as a plasma-facing material have been recently initiated [1–5]. In previous studies [1,2,5], sputtering properties of RAFM steel by deuterium (D) plasma were explored, using EUROFER, F82H, and Fe-W layers as a surrogate. The sputtering yields, inferred from mass loss, were found to decrease with an increase in D^+ fluence because of W enrichment on the surface, likely due to preferential sputtering of the lower *Z* elements. Since the sputtering yields were determined only from mass loss, details such as the time evolution of sputtered flux of each element and the elemental composition of the sputtered flux remain unclear.

Optical emission spectroscopy has been commonly used to investigate sputtering properties of plasma-facing materials. Line-of-sight integrated emission intensity of sputtered atoms, I_a, can be converted into sputtered atomic flux, Γ_{spt}, [6] with the parameter *S/XB* defined by,

$$\Gamma_{spt} = 4\pi \frac{S}{XB} I_a. \quad (1)$$

Here, *S* and *X* are the ionization and excitation rate coefficients, and *B* is the branching ratio. It is noted that this relation is valid only when the geometrical loss flux from the observation volume is negligible. The main elements in RAFM steel are iron (Fe), chromium (Cr), and tungsten (W). The atomic fraction of each element can vary somewhat depending on the specific steel being investigated, as mentioned below. Thus, *S/XB* values of these elements are necessary to quantify Γ_{spt} from the surface of RAFM steel. Both experimental [7–11] and theoretical [12] values of *S/XB* are available for W. The ADAS database [13] provides theoretical values of *S/XB* for Cr I lines, while no experimental verification has been done. For Fe I lines, neither experimental nor theoretical data are available. To address this need, we report the first *S/XB* values of both Fe I and Cr I lines (Section 3) using the technique developed in Ref. [14]. The sputtering properties of F82H and CLF-1 RAFM steels are further investigated with these experimentally

* Corresponding author.
E-mail address: dnishijima@eng.ucsd.edu (D. Nishijima).

http://dx.doi.org/10.1016/j.nme.2016.08.019

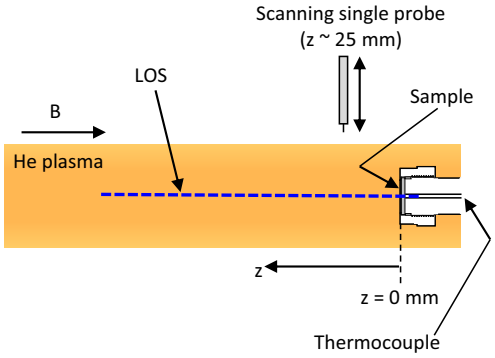

Fig. 1. Schematic view of the PISCES-B target region. The target surface is defined as $z = 0$ mm. The line-of-sight (LOS) of the spectroscopic system is indicated with the horizontal dashed line. The reciprocating single probe system is located at $z \sim 25$ mm.

determined *S/XB* values of Fe I and Cr I lines. The sputtered flux of each species is quantified during the course of plasma exposures. The time- (He^+ fluence-) integrated sputtering yields are compared with those from the mass loss technique. Furthermore, the sample temperature, T_s, dependence of the sputtering yield is explored in the range of $T_s \sim 573$–1053 K. Surface analyses are also conducted to support the spectroscopic data.

2. Experimental setup

The experiments were performed in the PISCES-B linear plasma device [15], the target region of which is schematically presented in Fig. 1. The background pressure was around 1×10^{-8} Torr for these experiments. All plasma exposures were done with a working gas of He at ~3 mTorr. Axial profiles of line emission intensities from sputtered particles and background He plasma were measured in front of the target surface ($z = 0$ mm). The spectroscopic line-of-sight is shown with a thick dashed line. A 0.5 m Czerny-Turner type spectrometer (Acton SP2560) is used with a 2-D CCD camera detector (Princeton Instruments PIXIS:400B). Plasma light emission is delivered to the entrance slit of the spectrometer via a plane mirror, a Dove prism, and a focusing lens. The Dove prism is employed to rotate the plasma image to align the plasma axis with the entrance slit. The plasma column spatial resolution is 1.34 mm per CCD channel. The ion flux, Γ_i, the electron density, n_e, and temperature, T_e, are measured with a reciprocating single Langmuir probe system located at $z \sim 25$ mm. The incident ion energy, E_i, is controlled by negatively biasing the target, V_t, with respect to the plasma space potential, V_s, which is also obtained with the single probe. The sample temperature, T_s, is measured with a thermocouple attached to the rear of the sample, and is controlled with forced air cooling.

Disk F82H samples with a diameter of 25 mm and a thickness of 1.5 mm were made of a plate [F82H-IEA (Heat#9741) Plate ID 2–20], supplied from QST, Japan. The surface of F82H samples was sanded (150 grit). Mirror-polished CLF-1 disk samples (25 mm diameter and 1 mm thickness) were provided by ASIPP, China. This grade has been developed by SWIP, China, for Chinese TBM (test blanket module) in ITER. The nominal bulk composition of F82H and CLF-1 is Fe-8Cr-2 W and Fe-8.5Cr-1.5 W in wt% for the main elements, respectively. Although oxide layers are formed on the surface, those are quickly removed under the high flux plasma exposure [16].

Before and after the plasma exposures, the surface composition was measured with Auger electron spectroscopy (AES) before exposing the samples to air. A scanning electron microscope (SEM) was used to observe surface morphology. The samples were

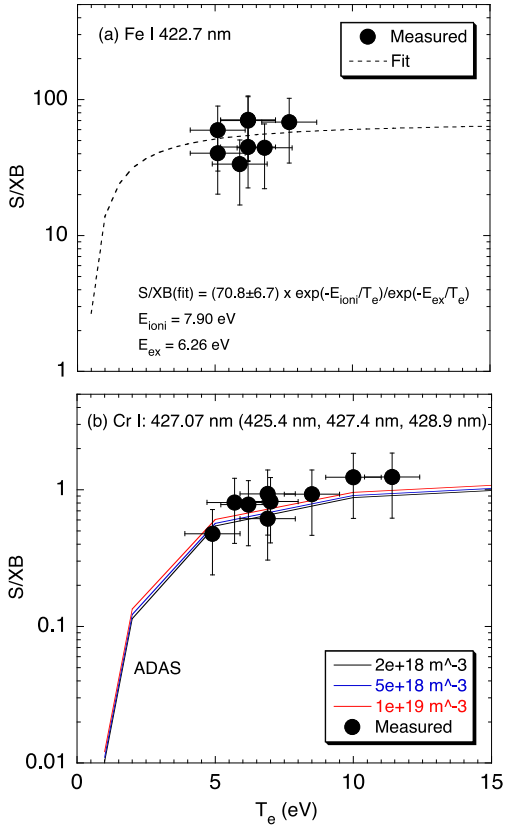

Fig. 2. *S/XB* values of (a) Fe I 422.7 nm and (b) Cr I 427.1 nm (425.4, 427.4, and 428.9 nm). Closed circles show measured values in this experiment. In (a), a fitted curve is shown with a dashed line, while ADAS data (llu) are presented with solid lines at different n_e in (b).

weighed before and after plasma exposure with a microbalance (10 μg resolution) to derive the mass loss. For comparison with spectroscopy, the sputtering yield is calculated with the mass loss and the incident ion fluence from single probe measurements.

3. *S/XB* measurements of Fe I and Cr I lines

S/XB values of an Fe I 422.7 nm line and a multiplet-averaged Cr I 427.1 nm line (425.4, 427.4, and 428.9 nm) are experimentally determined using the technique described in Ref. [14]. Here, only a brief explanation is given.

From Eq. (1), $S/XB = \Gamma_{spt}/(4\pi I_a) = (Y\Gamma_i)/(4\pi I_a)$ is derived, where Y is the sputtering yield. The sputtering yield of Fe and Cr bombarded by He at $E_i \sim 80$ eV was determined to be $\sim(1.5 \pm 0.3) \times 10^{-3}$ and $\sim(3.0 \pm 0.6) \times 10^{-3}$, respectively, from mass loss in a dedicated plasma exposure to each pure material. The line emission intensity of sputtered Fe/Cr atoms from each pure material was measured during various plasma conditions, and converted into the local emissivity, simply divided by the horizontal length of the emission zone (10 mm) [14]. The local emissivity was then axially integrated to obtain the total intensity, I_a. At each condition, the incident ion flux, Γ_i, as well as T_e were evaluated with the single probe. In this way, *S/XB* values of Fe I and Cr I lines are determined using only measured parameters.

The measured *S/XB* values of Fe I 422.7 nm are plotted against T_e in Fig. 2(a). Since there is no theoretical data available for Fe, the experimental data is fit to a simple function, $S/XB = \beta \times \exp(-E_{ioni}/T_e)/\exp(-E_{ex}/T_e)$, with the ionization energy ($E_{ioni} = 7.90$ eV) of Fe, the excitation energy ($E_{ex} = 6.26$ eV) of the upper state, and β a fitting parameter. This fit function is a natural choice from the definition of *S/XB*. Because of the proximity between E_{ioni} and E_{ex},

Please cite this article as: D. Nishijima et al., Sputtering properties of RAFM steels under high-flux He plasma exposure, Nuclear Materials and Energy (2016), http://dx.doi.org/10.1016/j.nme.2016.08.019

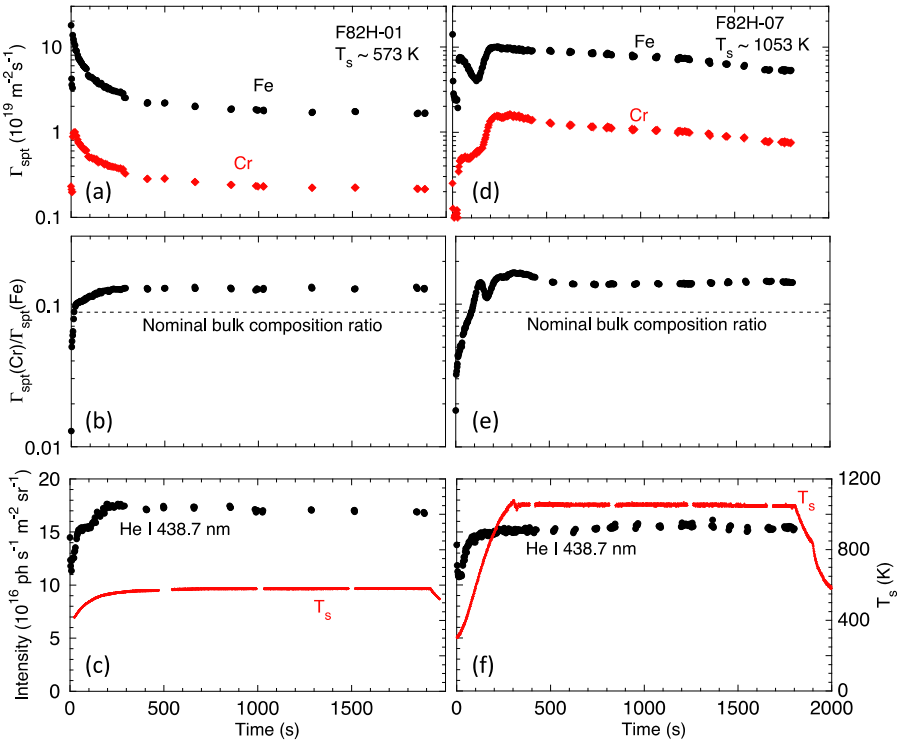

Fig. 3. Time evolution of (a) and (d) Γ_{spt}(Fe) and Γ_{spt}(Cr), (b) and (e) Γ_{spt}(Cr)/Γ_{spt}(Fe), (c) and (f) the He I 438.7 nm line intensity and T_s, during He plasma exposure to F82H samples. (a)-(c): F82H-01 at $T_s \sim 573$ K. (d)-(f): F82H-07 at $T_s \sim 1053$ K.

the fit function is nearly flat at $T_e \geq 2$ eV, and the measured data also show the weak T_e dependence. The nonlinear curve fit gives $\beta = 70.8 \pm 6.7$, where the uncertainties of the measured data were not taken into account in the fit. Fig. 2(b) shows good agreement of the T_e dependence of Cr I 427.1 nm *S/XB* values between experimental and ADAS theoretical data [13].

The ionization mean free path, λ_{mfp}, for all the data in Fig. 2 is evaluated to be $\leq$10 mm from an exponential fit to the observed axial intensity profile. This confirms that most of sputtered atoms are ionized in the plasma column, i.e. the geometrical loss flux is negligibly small [14].

4. Sputtering behavior of RAFM steels

In this section, sputtering behavior of RAFM steels exposed to He plasmas with $\Gamma_i \sim (2\text{–}4) \times 10^{22}$ m^{-2}s^{-1} and $E_i \sim 80$ eV is investigated in the range of $T_s \sim 573\text{–}1053$ K. In addition to spectroscopy during plasma exposure, mass loss measurements and post-mortem surface analyses (AES and SEM) were performed.

In Fig. 3, the time evolution of sputtered fluxes of Fe, Γ_{spt}(Fe), and Cr, Γ_{spt}(Cr), from F82H evaluated with spectroscopy is presented for two different flat-topped T_s cases: (a) ~573 K and (b) ~1053 K. The plasma discharge started with $V_t = -60$ V to avoid arcing on the target surface, and V_t was then increased from −60 V to −90 V ($E_i \sim 80$ eV) during the first ~10–20 s, so that Γ_{spt} is lower at the beginning. As shown with the He I 438.7 nm line intensity in Fig. 3(c) and (f), the plasma reached the steady state condition within ~100–200 s. It should be first noted that no W I lines were observed in this experiment, indicating that W was not sputtered because of the low E_i. This means that Fe and Cr are preferentially sputtered. At $T_s \sim 573$ K, both Γ_{spt}(Fe) and Γ_{spt}(Cr) are found to rapidly drop with increasing the plasma exposure time, i.e. the He^+ fluence, by a factor of ~5–8, and to reach the saturation level within 1000 s. On the other hand, during the ramp-up phase of T_s for the high T_s case (1053 K), there is a minimum of Γ_{spt}(Fe), while Γ_{spt}(Cr) increases with an increase in T_s. After having a maximum of Γ_{spt}(Fe) and Γ_{spt}(Cr), those slowly decrease without reaching the saturation until the end of the discharge. The sputtered flux ratio, Γ_{spt}(Cr)/ Γ_{spt}(Fe), is plotted in Fig. 3(b) and (e). In both cases, the ratio is higher than the nominal bulk composition ratio (~0.088), indicating that the diffusion of Cr to the surface is faster than that of Fe.

To compare the spectroscopic and mass loss measurements, the time-integrated sputtering yield of F82H is obtained from both methods in several plasma exposures. For spectroscopy, Γ_{spt}(Fe) and Γ_{spt}(Cr) are time-integrated to derive the total number of sputtered atoms over the plasma exposure. The time-integrated sputtering yield of F82H is calculated by dividing the total number of sputtered Fe and Cr atoms by the number of incident He^+ ions. The number of sputtered atoms from mass loss is calculated

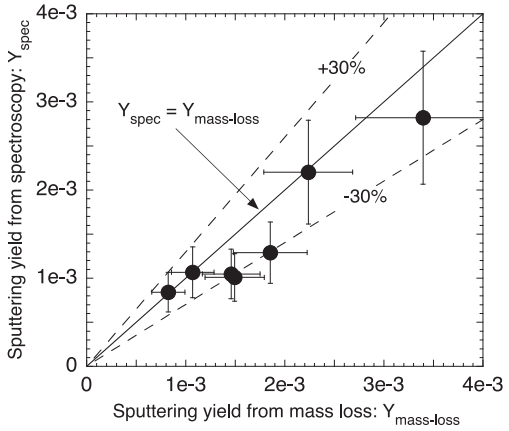

Fig. 4. Comparison of the time- (fluence-) integrated F82H sputtering yields between the spectroscopic (Y_{spec}) and mass loss ($Y_{mass\text{-}loss}$) techniques.

Please cite this article as: D. Nishijima et al., Sputtering properties of RAFM steels under high-flux He plasma exposure, Nuclear Materials and Energy (2016), http://dx.doi.org/10.1016/j.nme.2016.08.019

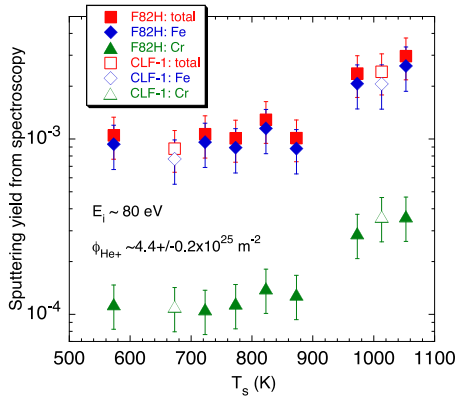

Fig. 5. T_s dependence of the fluence-integrated sputtering yields of total (squares), Fe (diamonds), and Cr (triangles) obtained from spectroscopy. The sputtering yield of F82H (closed symbols) agrees well with that of CLF-1 (open symbols) in this T_s range. $E_i \sim 80$ eV and $\phi_{He+} \sim 4.4+/-0.2 \times 10^{25}$ m^{-2}.

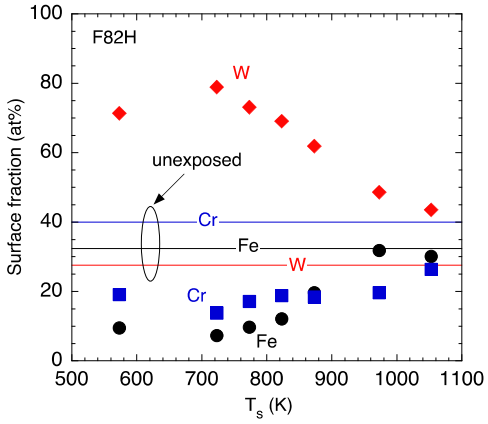

Fig. 6. Surface fractions of Fe (circles), Cr (squares), and W (diamonds) as a function of T_s measured with AES after He plasma exposure of F82H. Solid lines show the surface composition of an unexposed F82H surface, which was also measured with AES.

with the effective atomic mass (~55.5 amu) evaluated from spectroscopy. As presented in Fig. 4, the sputtering yield from spectroscopy is in good agreement with that from mass loss (within 30%). It should be noted that this good agreement verifies that our measured *S/XB* values are valid.

Fig. 5 shows the T_s dependence of the time- (fluence-) integrated sputtering yields of Fe, Cr, and the total, i.e. F82H, from spectroscopy at an incident He^+ ion fluence $\phi_{He+} \sim 4.4 \pm 0.2 \times 10^{25}$ m^{-2}. The sputtering yield of F82H (closed symbols) is dominated by Fe, as expected from Fig. 3. The sputtering yield is found to be constant up to $T_s \sim 900$ K, and to be enhanced at $T_s > 900$ K. Data from CLF-1 are also plotted (open symbols). While the surface preparation is different between two steels, the sputtering yield is found to be very similar because the plasma exposure induces the development of surface morphology, as described later.

Both the sputtering yield reduction during the plasma exposure (Fig. 3) and the T_s dependence of the sputtering yield (Fig. 5) can be explained by the following two effects: (1) the surface enrichment of W due to the preferential sputtering of Fe and Cr, and (2) the surface morphology development. The preferential sputtering of Fe and Cr is confirmed with spectroscopic observations (Fig. 3). The resultant enrichment of W on the surface is observed with AES. Fig. 6 presents the surface fractions of Fe, Cr, and W after the He plasma exposure to F82H at $T_s \sim 573$–1053 K, compared to those of an unexposed surface. Since Fe may be preferentially removed by sanding, the surface composition of the unexposed surface strongly deviates from the bulk composition. The enrichment of W as well as the depletion of Fe and Cr are clearly seen, especially, at $T_s < 900$ K. The W enrichment is reduced at $T_s > 900$ K due presumably to the enhanced diffusion of Fe and Cr [17]. It should be noted that only Fe, Cr, and W are taken into account. We do not show low-level surface contaminants such as O and C, which were nevertheless also observed.

SEM images of He plasma-exposed F82H surfaces are shown in Fig. 7. High-density and nano-scale cone-like structures are seen at $T_s \sim 573$ K and 723 K. This kind of structure is known to reduce the erosion rate [16,18], because of the direct line-of-sight deposi-

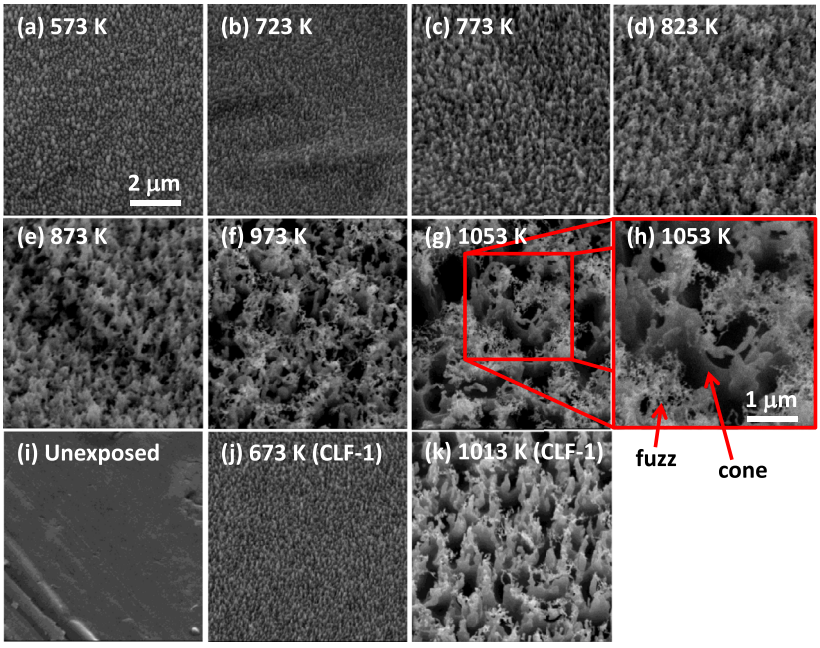

Fig. 7. SEM images of (a)-(h) He plasma-exposed F82H surfaces at $T_s \sim 573$–1053 K, (i) an unexposed F82H surface, and (j)-(k) He plasma-exposed CLF-1 surfaces at $T_s \sim 673$ K and 1013 K. The square region of (g) is enlarged in (h), denoting fuzz and cone. The observation angle is 45° with respect to the surface normal.

Please cite this article as: D. Nishijima et al., Sputtering properties of RAFM steels under high-flux He plasma exposure, Nuclear Materials and Energy (2016), http://dx.doi.org/10.1016/j.nme.2016.08.019

tion of sputtered atoms. Here, only atoms released into the plasma are included in the erosion rate. Cones become larger with increasing T_s, but smaller scale structures seem to grow on top of the cones. At $T_s \geq 973$ K, fuzzy structures [19,20] clearly appear on top of the cone-like structures. To identify the composition of the fuzz, it was collected with carbon tape. It is found from EDX (energy-dispersive X-ray spectroscopy) measurements that W is the dominant element of the fuzz: ~61–62 at% of W, ~31–32 at% of Fe, and ~7 at% of Cr. Comparing the 973 K and 1053 K cases, the base cone-like structures are larger and the density of W fuzz is lower at $T_s \sim 1053$ K. This is consistent with the higher sputtering yield (Fig. 5) and the lower W surface concentration (Fig. 6).

Concerning CLF-1, the surface composition after the plasma exposure is consistent with that of F82H at $T_s \sim 673$ K, while the W fraction is slightly lower for CLF-1 by ~10 at% at $T_s \sim 1013$ K. The surface morphology looks very similar to that of F82H at $T_s \sim 673$ K. As seen in Fig. 7(k), W-rich fuzz also develops on the CLF-1 surface at $T_s \sim 1013$ K, but is less prevalent compared to F82H, which is consistent with the AES measurements. Regardless of the slightly different surface composition and morphology of CLF-1, the sputtering yield is consistent with F82H within the uncertainties (see Fig. 5).

5. Conclusion

S/XB values of Fe I and Cr I lines are experimentally determined for the first time, enabling the study of the sputtering properties of F82H and CLF-1 RAFM steels with optical spectroscopy. The erosion rates obtained from spectroscopy using the determined *S/XB* values are in good agreement with those from mass loss. This confirms the validity of the measured *S/XB* values. High-flux He plasma exposure at low $E_i \sim 80$ eV leads to preferential sputtering of Fe and Cr, and thus to surface enrichment of W. Interestingly, high temperature exposures at $T_s \geq 973$ K result in the formation of W-rich fuzz on top of the cone-like structures. Both the surface enrichment of W and the development of surface morphology contribute to the reduction of the sputtering yield of the RAFM steels. In future fusion devices, should RAFM steel be used as a first wall, T_s will need to be kept below 900 K from the sputtering point of view, as the sputtering yield increases at ~900 K. Further investigation, however, must be done.

Acknowledgements

We appreciate the PISCES technical staff and beryllium personnel for their devoted work. This work is supported by the US DOE Grant: DE-FG02-07ER54912, and is conducted as part of IAEA CRP on Plasma-wall Interaction with Reduced-activation Steel Surfaces in Fusion Devices.

References

[1] J. Roth, et al., J. Nucl. Mater. 454 (2014) 1.
[2] K. Sugiyama, et al., J. Nucl. Mater. 463 (2015) 272.
[3] V.Kh. Alimov, et al., Phys. Scr. T159 (2014) 014049.
[4] K. Yakushiji, et al., Phys. Scr. T167 (2016) 014067.
[5] V.Kh. Alimov, et al., Nucl. Mater. Energy 7 (2016) 25.
[6] K.H. Behringer, J. Nucl. Mater. 145-147 (1987) 145.
[7] J. Steinbrink, et al., in: Proc. 24th EPS Conf. on Controlled Fusion and Plasma Physics, 21A, Berchtesgaden, Germany, 1997, p. 1809.
[8] A. Geier, et al., Rev. Sci. Instrum. 70 (1999) 63.
[9] A. Geier, et al., Plasma Phys. Control. Fusion 44 (2002) 2091.
[10] D. Nishijima, et al., Phys. Plasmas 16 (2009) 122503.
[11] D. Nishijima, et al., Phys. Plasmas 18 (2011) 019901.
[12] I. Beigman, et al., Plasma Phys. Control. Fusion 49 (2007) 1833.
[13] H.P. Summers, The ADAS User Manual version 2.6 (2004).
[14] D. Nishijima, et al., J. Nucl. Mater. 438 (2013) S1245.
[15] R.P. Doerner, et al., Phys. Scr. T111 (2004) 75.
[16] R.P. Doerner, et al., J. Nucl. Mater. 438 (2013) S272.
[17] U. von Toussaint, et al., Phys. Scr. T167 (2016) 014023.
[18] R.P. Doerner, et al., J. Nucl. Mater. 455 (2014) 1.
[19] M.J. Baldwin, R.P. Doerner, Nucl. Fusion 48 (2008) 035001.
[20] S. Kajita, et al., Nucl. Fusion 49 (2009) 095005.